Inorg. Chem. **2008**, *47*, 5234−5244

Preparation and Structural Characterization of the I_h and the D_{5h} Isomers of the Endohedral Fullerenes $Tm_3N@C_{80}$: Icosahedral C_{80} Cage Encapsulation of a Trimetallic Nitride Magnetic Cluster with Three Uncoupled Tm^{3+} Ions

Tianming Zuo,[†] Marilyn M. Olmstead,[‡] Christine M. Beavers,[‡] Alan L. Balch,*[,‡] Guangbin Wang,[†] Gordon T. Yee,[†] Chunying Shu,[†] Liaosa Xu,[†] Bevan Elliott,[§] Luis Echegoyen,[§] James C. Duchamp,[||] and Harry C. Dorn*[,†]

Chemistry Departments, Virginia Polytechnic Institute and State University, Blacksburg, Virginia 24061, University of California, Davis, California 95616, Clemson University, Clemson, South Carolina 29634, and Emory and Henry College, Emory, Virginia 24327

Received February 13, 2008

We report an efficient method for the preparation and purification of the I_h and the D_{5h} isomers of $Tm_3N@C_{80}$. Following preparation in a Krätschmer−Huffman electric-arc generator, the $Tm_3N@C_{80}$ isomers were obtained by a chemical separation process followed by a one-stage isomer selective chromatographic high-performance liquid chromatography (HPLC) separation (pyrenyl, 5PYE column). The HPLC chromatographic retention behavior on a pentabromobenzyl (5PBB) column suggests a charge transfer of ∼6 electrons; $[M_3N]^{6+}@C_{80}^{6-}$ and the chromatographic retention mechanisms of the I_h and the D_{5h} isomers of $Tm_3N@C_{80}$ on both 5PBB and 5PYE columns are discussed. Single-crystal X-ray diffraction data demonstrate that the Tm_3N cluster has a planar structure but represents a tight fit for trapping the Tm_3N cluster inside the I_h- and the D_{5h}-C_{80} cages. Specifically, the Tm atoms punch out the cage carbon atoms adjacent to them. The "punched out" effect can be demonstrated by cage radii and pyramidal angles at cage carbon atoms near the Tm atoms. The magnetic susceptibility (χT) for $Tm_3N@I_h$-C_{80} was found to exhibit Curie−Weiss behavior with $C = 23.4$ emu·K/mol, which is consistent with the calculated value for three uncoupled Tm^{3+} ions by considering the spin and orbital contributions with no quenching of the orbital angular momentum ($L = 5$, $S = 1$, and $J = 6$; $C_{calcd} = 23.3$ emu·K/mol). The electrochemical measurements demonstrate that both the I_h and the D_{5h} isomers of $Tm_3N@C_{80}$ have a large electrochemical gap.

Introduction

Endohedral fullerenes are neutral molecules that consist of a closed cage of carbon atoms, which encapsulates one or more heteroatoms or molecules.[1] There has been considerable current interest in the preparation and the properties of new endofullerenes.[2−7] While it is possible to insert atoms or small molecules into preformed empty-cage fullerenes by creating openings in the fabric of the fullerene,[8,9] the majority of endofullerenes are prepared by a modification of the Krätschmer−Huffman electric-arc process.[10] In this modified process, graphite and a metal oxide are covaporized in a low-pressure helium atmosphere to produce a black soot that

* To whom correspondence should be addressed. E-mail: hdorn@vt.edu (H.C.D.), albalch@ucdavis.edu (A.L.B.). Fax: (540) 231-3255.
[†] Virginia Polytechnic Institute and State University.
[‡] University of California, Davis.
[§] Clemson University.
[||] Emory and Henry College.

(1) Akasaka, T.; Nagase, S. *Endofullerenes: A New Family of Carbon Clusters (Developments in Fullerene Science)*; Kluwer Academic Publishers: Dordrecht, The Netherlands, 2002.
(2) Beavers, C. M.; Zuo, T.; Duchamp, J. C.; Harich, K.; Dorn, H. C.; Olmstead, M. M.; Balch, A. L. *J. Am. Chem. Soc.* **2006**, *128*, 11352–11353.
(3) Echegoyen, L.; Chancellor, C. J.; Cardona, C. M.; Elliott, B.; Rivera, J.; Olmstead, M. M.; Balch, A. L. *Chem. Commun.* **2006**, 2653–2655.
(4) Wakahara, T.; Yamada, M.; Takahashi, S.; Nakahodo, T.; Tsuchiya, T.; Maeda, Y.; Akasaka, T.; Kako, M.; Yoza, K.; Horn, E.; Mizorogi, N.; Nagase, S. *Chem. Commun.* **2007**, 2680–2682.
(5) Wakahara, T.; Nikawa, H.; Kikuchi, T.; Nakahodo, T.; Rahman, G. M. A.; Tsuchiya, T.; Maeda, Y.; Akasaka, T.; Yoza, K.; Horn, E.; Yamamoto, K.; Mizorogi, N.; Slanina, Z.; Nagase, S. *J. Am. Chem. Soc.* **2006**, *128*, 14228–14229.
(6) Murata, Y.; Murata, M.; Komatsu, K. *J. Am. Chem. Soc.* **2003**, *125*, 7152–7153.
(7) Iiduka, Y.; Wakahara, T.; Nakahodo, T.; Tsuchiya, T.; Sakuraba, A.; Maeda, Y.; Akasaka, T.; Yoza, K.; Horn, E.; Kato, T.; Liu, M. T. H.; Mizorogi, N.; Kobayashi, K.; Nagase, S. *J. Am. Chem. Soc.* **2005**, *127*, 12500–12501.

10.1021/ic800227x CCC: $40.75

Published on Web 04/30/2008

contains an array of empty-cage fullerenes and endofullerenes. The endofullerenes that result may contain from one to four electropositive metal atoms in carbon cages of various sizes, but these endofullerenes are usually formed in very low yield.[1] However, in 1999, the discovery was made that a new class of endofullerenes (e.g., $Sc_3N@C_{80}$,[11] $Sc_3N@C_{78}$,[12] and $Sc_3N@C_{68}$[13,14]) containing the M_3N group can be prepared in significantly higher yield by conducting the modified Krätschmer−Huffman arc process in the presence of dinitrogen. This development has made the $M_3N@C_{2n}$ group of endofullerenes available in sufficient quantities to allow the exploration of their chemical and physical properties.

Generally, conducting the Krätschmer−Huffman arc process in the presence of dinitrogen produces the 80-carbon cage endofullerene, $M_3N@C_{80}$, in the highest yield. In many cases, two cage isomers of $M_3N@C_{80}$ with I_h and D_{5h} symmetry are produced with the I_h isomer predominating.[15–17] This process also allows a wide range of metal ions including those of group 3B and the lanthanides to be placed inside the cage. Since it is well-known that fullerene cages are readily reduced, the electronic distribution within the $M_3N@C_{80}$ molecule is widely believed to involve the metals in their usual M(III) oxidation state, a central nitride ion (N^{3-}), and a carbon cage bearing a formal −6 charge. Detailed single-crystal X-ray structural information about lanthanide containing molecules of the type $M_3N@C_{80}$ is available for $Gd_3N@I_h$-C_{80},[18,19] $Tb_3N@I_h$-C_{80},[20] $Dy_3N@I_h$-C_{80},[21] and $Lu_3N@I_h$-C_{80}.[22] Additionally, mix-metal endofullerenes can also be prepared and purified. In this regard, crystallographic data are available for $CeSc_2@I_h$-C_{80}[23] and $Er_2Sc@I_h$-C_{80}.[24] Only one lanthanide complex, $Tb_3N@$ D_{5h}-C_{80}, containing the D_{5h}-C_{80} cage has been crystallographically characterized.[20]

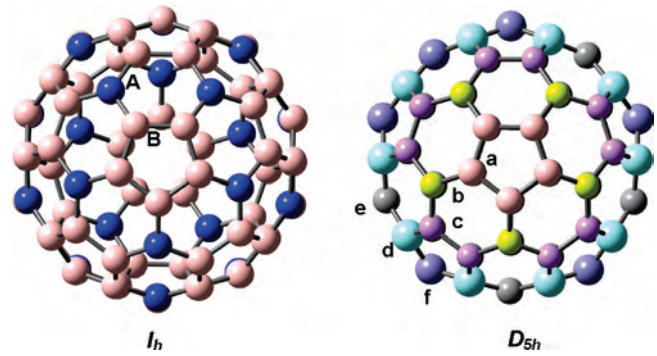

Figure 1. Illustration of the symmetry of the I_h and the D_{5h} isomers of C_{80} with labels for the different kinds of carbon atoms based on symmetry considerations. The I_h-C_{80} isomer can be obtained from the D_{5h} isomer by slicing the D_{5h} isomer along its horizontal mirror plane, rotating one-half by 36°, and putting the two halves back together.

Figure 1 shows comparative views down the 5-fold axes of the I_h- and D_{5h}-C_{80} fullerene cages. In the I_h isomer, there are only two different types of carbon atoms: those where three hexagons intersect (**A**) and those where two hexagons and a pentagon intersect (**B**). In the D_{5h} isomer, however, because of the lower symmetry, there are six different types of carbon atoms, which are labeled **a**−**f**.

The ability to incorporate a range of lanthanide ions into the $M_3N@C_{2n}$ class of endofullerenes allows the preparation of molecules with a wide, but controllable, variation in properties and potential uses.[25] For example, lanthanide ions can exhibit luminescence, variable degrees of paramagnetism, and high cross sections for absorption of X-rays, and these properties will become an intrinsic feature of the endofullerenes that contain these ions. Thus, luminescence has been observed for members of the metallofullerene family, $Er_xSc_{3-x}N@C_{80}$.[26] The large magnetic moment of Gd(III) provides endofullerenes that have been shown to have high relaxivities and to provide a promising new generation of contrast agents for magnetic resonance imaging (MRI).[27–32] Additionally, $Lu_3N@C_{80}$ has been shown to act as an effective X-ray contrast agent.[33]

(8) Komatsu, K.; Murata, M.; Murata, Y. *Science* **2005**, *307*, 238–240.
(9) Saunders, M.; Cross, R. J.; Jimenez Vazquez, H. A.; Shimshi, R.; Khong, A. *Science* **1996**, *271*, 1693–1697.
(10) Krätschmer, W.; Lamb, L. D.; Fostiropoulos, K.; Huffman, D. R. *Nature* **1990**, *347*, 354–358.
(11) Stevenson, S.; Rice, G.; Glass, T.; Harlch, K.; Cromer, F.; Jordan, M. R.; Craft, J.; Hadju, E.; Bible, R.; Olmstead, M. M.; Maltra, K.; Fisher, A. J.; Balch, A. L.; Dorn, H. C. *Nature* **1999**, *401*, 55–57.
(12) Olmstead, M. M.; De Bettencourt-Dias, A.; Duchamp, J. C.; Stevenson, S.; Marciu, D.; Dorn, H. C.; Balch, A. L. *Angew. Chem., Int. Ed.* **2001**, *40*, 1223–1225.
(13) Stevenson, S.; Fowler, P. W.; Heine, T.; Duchamp, J. C.; Rice, G.; Glass, T.; Harich, K.; Hajdu, E.; Bible, R.; Dorn, H. C. *Nature* **2000**, *408*, 427–428.
(14) Olmstead, M. M.; Lee, H. M.; Duchamp, J. C.; Stevenson, S.; Marciu, D.; Dorn, H. C.; Balch, A. L. *Angew. Chem., Int. Ed.* **2003**, *42*, 900–903.
(15) Duchamp, J. C.; Demortier, A.; Fletcher, K. R.; Dorn, D.; Iezzi, E. B.; Glass, T.; Dorn, H. C. *Chem. Phys. Lett.* **2003**, *375*, 655–659.
(16) Krause, M.; Dunsch, L. *ChemPhysChem* **2004**, *5*, 1445–1449.
(17) Cai, T.; Xu, L.; Anderson, M. R.; Ge, Z.; Zuo, T.; Wang, X.; Olmstead, M. M.; Balch, A. L.; Gibson, H. W.; Dorn, H. C. *J. Am. Chem. Soc.* **2006**, *128*, 8581–8589.
(18) Stevenson, S.; Phillips, J. P.; Reid, J. E.; Olmstead, M. M.; Rath, S. P.; Balch, A. L. *Chem. Commun.* **2004**, 2814–5.
(19) Krause, M.; Dunsch, L. *Angew. Chem., Int. Ed.* **2005**, *44*, 1557–1560.
(20) Zuo, T.; Beavers, C. M.; Duchamp, J. C.; Campbell, A.; Dorn, H. C.; Olmstead, M. M.; Balch, A. L. *J. Am. Chem. Soc.* **2007**, *129*, 2035–2043.
(21) Yang, S.; Troyanov, S. I.; Popov, A. A.; Krause, M.; Dunsch, L. *J. Am. Chem. Soc.* **2006**, *128*, 16733–16739.
(22) Stevenson, S.; Lee, H. M.; Olmstead, M. M.; Kozikowski, C.; Stevenson, P.; Balch, A. L. *Chem.−Eur. J.* **2002**, *8*, 4528–4535.
(23) Wang, X.; Zuo, T.; Olmstead, M. M.; Duchamp, J. C.; Glass, T. E.; Cromer, F.; Balch, A. L.; Dorn, H. C. *J. Am. Chem. Soc.* **2006**, *128*, 8884–8889.
(24) Olmstead, M. M.; de Bettencourt-Dias, A.; Duchamp, J. C.; Stevenson, S.; Dorn, H. C.; Balch, A. L. *J. Am. Chem. Soc.* **2000**, *122*, 12220–12226.
(25) Dorn, H. C.; Iezzi, E. B.; Stevenson, S.; Balch, A. L.; Duchamp, J. C. In *Endofullerenes: A New Family of Carbon Clusters*; Akasaka, T., Nagase, S., Eds.; Kluwer Academic Publishers: Dordrecht, The Netherlands, 2002; pp 121−129.
(26) MacFarlane, R. M.; Bethune, D. S.; Stevenson, S.; Dorn, H. C. *Chem. Phys. Lett.* **2001**, *343*, 229–234.
(27) Fatouros, P. P.; Corwin, F. D.; Chen, Z.-J.; Broaddus, W. C.; Tatum, J. L.; Kettenmann, B.; Ge, Z.; Gibson, H. W.; Russ, J. L.; Leonard, A. P.; Duchamp, J. C.; Dorn, H. C. *Radiology* **2006**, *240*, 756–764.
(28) Miyamoto, A.; Okimoto, H.; Shinohara, H.; Shibamoto, Y. *Eur. Radiol.* **2006**, *16*, 1050–1053.
(29) Tóth, E.; Bolskar, R. D.; Borel, A.; González, G.; Helm, L.; Merbach, A. E.; Sitharaman, B.; Wilson, L. J. *J. Am. Chem. Soc.* **2005**, *127*, 799–805.
(30) Bolskar, R. D.; Benedetto, A. F.; Husebo, L. O.; Price, R. E.; Jackson, E. F.; Wallace, S.; Wilson, L. J.; Alford, J. M. *J. Am. Chem. Soc.* **2003**, *125*, 5471–5478.
(31) Kato, H.; Kanazawa, Y.; Okumura, M.; Taninaka, A.; Yokawa, T.; Shinohara, H. *J. Am. Chem. Soc.* **2003**, *125*, 4391–4397.
(32) Mikawa, M.; Kato, H.; Okumura, M.; Narazaki, M.; Kanazawa, Y.; Miwa, N.; Shinohara, H. *Bioconjugate Chem.* **2001**, *12*, 510–514.

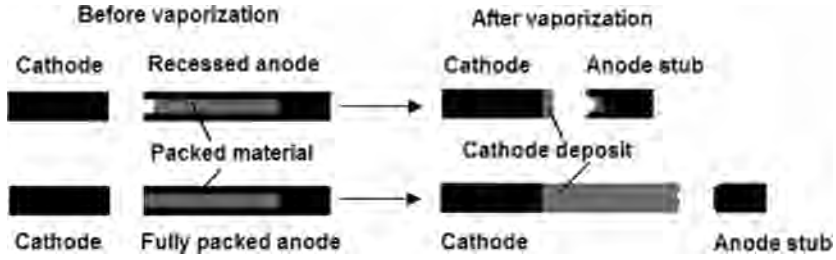

Figure 2. Illustration of alleviating the cathode deposit using a recessed anode.

Endofullerenes of the $M_3N@C_{80}$ type can contain three paramagnetic ions within a confined space where there is the potential for magnetic interaction between the individual metal ions. Because of the relevance to MRI, much of the work in this area has focused on the magnetic properties of gadolinium endofullerenes, but other lanthanium containing endofullerenes are also expected to display significant magnetic properties. Indeed, several computation studies have addressed the issue of the magnetic properties of $Gd_3N@I_h$-C_{80}.[34–36] Despite the fact that the 4f orbitals in lanthanides are highly contracted, magnetic coupling has been seen in dinuclear gadolinium(III) complexes and may occur with metal ions trapped inside fullerene cages.[37] However, relatively little experimental work has been conducted on the magnetic properties of the $M_3N@C_{80}$ endohedrals. Previously, Dunsch and co-workers reported the magnetic properties of $Ho_3N@C_{80}$ and $Tb_3N@C_{80}$.[38] In this type of endofullerene, the magnetic behavior is derived solely from the metal ions present; the nitride ion and the C_{80}^{6-} portions are diamagnetic. Dunsch and co-workers examined extremely small samples ($\sim$50 μg) and concluded that the moments on the rare earth atoms are exchanged coupled along the Ln-N axes in an equilateral triangular pattern to give an overall moment roughly two-thirds of that expected for decoupled spins.

Dunsch and co-workers have recently also reported the preparation and isolation of two isomers of $Tm_3N@C_{80}$ along with $Tm_3N@C_{82}$, $Tm_3N@C_{84}$, $Tm_3N@C_{86}$, and $Tm_3N@C_{88}$ via the modified Krätschmer−Huffman electric-arc process conducted in an atmosphere of helium and ammonia.[39,40] Ammonia served as the source of the nitride ion and suppressed the formation of C_{60} and C_{70}. The isomers of $Tm_3N@C_{80}$ were characterized by ultraviolet−visible (UV−vis), Fourier transform infrared (FTIR), Raman, and X-ray photoelectron (XPS) spectroscopies and by cyclic voltametry. However, the structure and magnetic properties of the two isomers of $Tm_3N@C_{80}$ have not been reported.

In this paper, we report on the formation of two isomers of $Tm_3N@C_{80}$ via an electric-arc process utilizing dinitrogen as the source of the nitride ion and a new combined chemical separation and chromatographic approach for preparing very pure samples of the I_h and the D_{5h} isomers of $Tm_3N@C_{80}$. We present the single-crystal X-ray diffraction structures and the electrochemical measurements for these isomers and examine the magnetic properties of $Tm_3N@I_h$-C_{80}.

Results and Discussion

Synthesis of $Tm_3N@C_{80}$. To prepare the $Tm_3N@C_{80}$ isomers, core-drilled quarter inch graphite rods (6.4 mm in diameter and 153 mm in length) were packed with a mixture of thulium oxide (Tm_2O_3), graphite powder, and iron nitride (Fe_xN, $x = 2\sim4$). The total Tm/C molar ratios were about 3:100. The packed rods were preheated at about 1000 °C under N_2 flow for about 10 h to remove air and moisture.[41] The rods were then vaporized in a Krätschmer−Huffman arc-discharge fullerene generator filled with a mixture of 20 torr dinitrogen and 280 torr helium gases. We have found that static vaporization (no He gas flow during vaporization) provides a higher total yield of the Tm-based endofullerenes and uses much less dinitrogen and helium gases. Because of its lower boiling point and the narrow liquid range, Tm metal appears to readily escape from the fullerene formation zone in the plasma and leads to deposits on the cathode. Therefore, the yields of the Tm-based endofullerenes are generally very low. The cathode deposit can cause an unstable plasma and can even extinguish the plasma. Consequently, much longer vaporization times are needed for the process. To help alleviate cathode deposit buildup, we found that a recessed anode rod (leaving $\sim$3 mm unpacked from the opening rim of the rod) can prevent the formation of the cathode deposit (see Figure 2). A possible advantage of the recessed anode results from the partial trapping of the plasma in the recessed empty part of the anode, which could provide a higher vaporization temperature for the rod-packed materials. With the current approach, the yield of the mixture of the $Tm_3N@C_{80}$ isomers is about 100−200 μg/quarter inch rod.

Separation of the I_h and the D_{5h} Isomers of $Tm_3N@C_{80}$. The soot from the electric-arc process was first extracted with refluxing toluene to yield a reddish-brown solution containing empty-cage fullerenes and endofullerenes, as illustrated in the high-performance liquid chromatography (HPLC) trace

(33) Iezzi, E. B.; Duchamp, J. C.; Fletcher, K. R.; Glass, T. E.; Dorn, H. C. *Nano Lett.* **2002**, *2*, 1187–1190.
(34) Lu, J.; Sabirianov, R. F.; Mei, W. N.; Gao, Y.; Duan, C. G.; Zeng, X. C. *J. Phys. Chem. B* **2006**, *110*, 23637–23640.
(35) Qian, M. C.; Khanna, S. N. *J. Appl. Phys.* **2007**, *101*, 09E105.
(36) Qian, M. C.; Ong, S. V.; Khanna, S. N.; Knickelbein, M. B. *Phys. Rev. B: Condens. Matter Mater. Phys.* **2007**, *75*, 104424.
(37) Roy, L. E.; Hughbanks, T. *J. Am. Chem. Soc.* **2006**, *128*, 568–575.
(38) Wolf, M.; Mueller, K.-H.; Skourski, Y.; Eckert, D.; Georgi, P.; Krause, M.; Dunsch, L. *Angew. Chem., Int. Ed.* **2005**, *44*, 3306–3309.
(39) Krause, M.; Liu, X.; Wong, J.; Pichler, T.; Knupfer, M.; Dunsch, L. *J. Phys. Chem. A* **2005**, *109*, 7088–7093.
(40) Krause, M.; Wong, J.; Dunsch, L. *Chem.—Eur. J.* **2005**, *11*, 706–11.
(41) Shinohara, H.; Hayashi, N.; Sato, H. *J. Phys. Chem.* **1993**, *97*, 13438–13440.

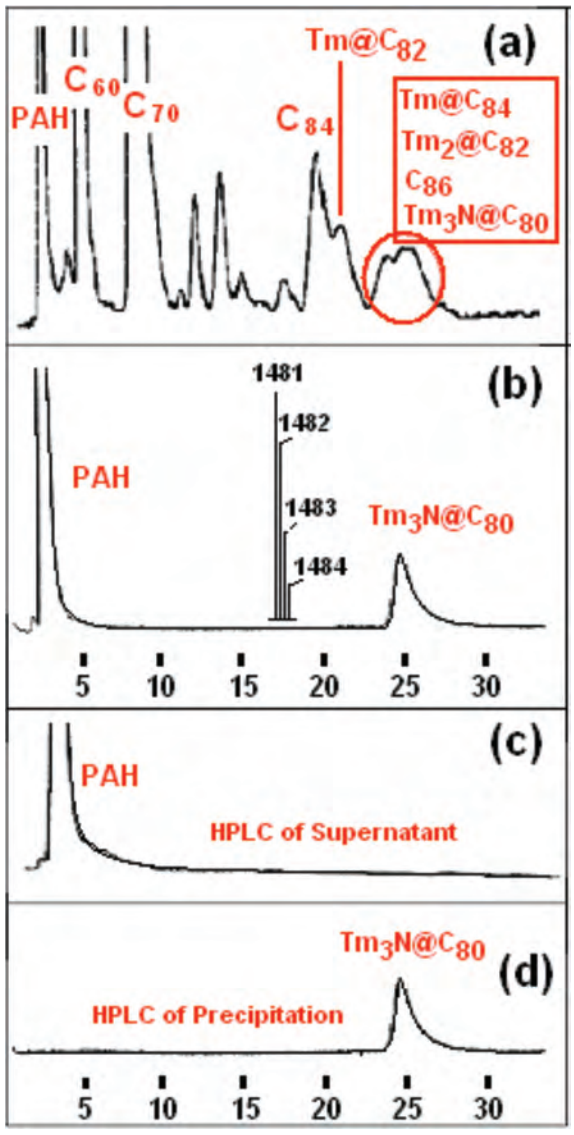

Figure 3. (a) HPLC chromatogram of the initial toluene extract. In this case, modest quantities of PAHs were observed because of the leakage of H_2O vapor (from the air) during preparation in our Krätschmer−Huffman generator. Even larger quantities of PAHs have been reported when NH_3 is used as the source of nitrogen.[40] (b) HPLC chromatogram of the material after elution through the CPDE-MPR column. The two peaks from left to right are due to PAHs and the $Tm_3N@C_{80}$ isomers, respectively. The insert shows the negative ion DCI MS spectrum of the sample, which corresponds to $Tm_3N@C_{80}$. (c) HPLC trace of the acetone solution (containing PAHs, redissolved in toluene) obtained from the centrifuge tube. (d) The HPLC trace of the precipitate ($Tm_3N@C_{80}$, redissolved in toluene) obtained from the centrifuge tube. The HPLC traces were obtained using a 5PBB column (4.6 mm × 250 mm). Toluene was the mobile phase with a flow rate of 2.0 mL/min. The detection wavelength was 390 nm.

in Figure 3a. The extract was initially separated utilizing a cyclopentadiene functionalized Merrifield peptide resin (CPDE-MPR) column, as previously described.[42,43] The first peak in Figure 3b is due to an aromatic hydrocarbon fraction commonly referred to as PAHs. The second peak is the desired mixture of $Tm_3N@C_{80}$ isomers. By comparing Figures 3a and 3b, it is clear that all of the empty cages and classical EMFs are retained on the CPDE-MPR column and only PAHs and $Tm_3N@C_{80}$ are eluted. The PAHs were subsequently removed using an acetone wash process followed by a centrifugation step, as illustrated in Figures 3c and 3d. From Figures 3c and 3d, it is clear that a purified fraction of $Tm_3N@C_{80}$ isomers can be achieved by this CPDE-MPR chemical separation and acetone washing process. The chemical separation approach relies on the inherent chemical kinetic stability of TNT EMFs relative to empty-cage fullerenes and non-TNT EMFs.[17]

Isolation of the I_h and the D_{5h} Isomers of $Tm_3N@C_{80}$. The HPLC peak for $Tm_3N@C_{80}$ (5PBB column) in Figure 3d is not symmetric, suggesting that the tailing edge of the peak could contain the second isomer of $Tm_3N@C_{80}$. The recovered sample was reinjected into a 5PYE column, and the smaller peak in Figure 4 was collected. Its MS spectrum (Figure 4b) has the same molecular weight (1481 amu) as $Tm_3N@C_{80}$; and therefore, it corresponds to another isomer of $Tm_3N@C_{80}$. After the isolation of the two isomers of $Tm_3N@C_{80}$, the HPLC chromatograms are shown in the insert part of Figure 4a. The ratio of peak areas for the two isomers of $Tm_3N@C_{80}$ is about 87:13, which is very similar to the corresponding ratio of I_h and D_{5h} isomers of $Sc_3N@C_{80}$.[17]

Characterization of the $Tm_3N@C_{80}$ Isomers. UV−Vis Spectra. The UV−vis spectra of the pure I_h and D_{5h} isomers of $Tm_3N@C_{80}$ in the carbon disulfide or toluene solution are shown in Figure 5. The absorption of the I_h isomer generally decreases from 400 nm to a longer wavelength, while the absorption of the D_{5h} isomer has a peak around 460 nm. These UV−vis absorption characteristics are nearly identical to those reported by Dunsch and co-workers for their samples of the isomers of $Tm_3N@C_{80}$ prepared under an atmosphere of ammonia.[39,40] Thus, while preparations of the endofullerenes under ammonia or under dinitrogen produce differing arrays of products, both methods yield the same two isomers of $Tm_3N@C_{80}$.

Chromatographic Capacity Factors for the I_h and the D_{5h} Isomers of $Tm_3N@C_{80}$. It is well-recognized that the capacity factor and the fullerene cage size have a simple linear relationship on most nonpolar columns. The retention mechanism is generally proportional to the fullerene cage polarizability and is dominated by $\pi-\pi$ interactions with the stationary phase.[44,45] As noted in Figure 6, the plots of log K versus cage size for empty-cage fullerenes are linear for both PBB and PYE columns. However, the PBB stationary phase has a higher slope than the PYE column with the same solvent (toluene) for the empty-cage fullerenes. Thus, coelution on the 5PBB column of the I_h and the D_{5h} isomers of $Tm_3N@C_{80}$ suggests that they have the same cage size (or polarizable π electrons). Figure 6a shows that the retention time for the I_h and the D_{5h} isomers of $Tm_3N@C_{80}$ corresponds to empty-cage C_{86} (~86 π electrons), although

(42) Ge, Z.; Duchamp, J. C.; Cai, T.; Gibson, H. W.; Dorn, H. C. *J. Am. Chem. Soc.* **2005**, *127*, 16292–16298.
(43) Guhr, K. I.; Greaves, M. D.; Rotello, V. M. *J. Am. Chem. Soc.* **1994**, *116*, 5997–5998.
(44) Fuchs, D.; Rietschel, H.; Michel, R. H.; Fischer, A.; Weis, P.; Kappes, M. M. *J. Phys. Chem.* **1996**, *100*, 725–729.
(45) Stevenson, S.; Burbank, P.; Harich, K.; Sun, Z.; Dorn, H. C.; van Loosdrecht, P. H. M.; deVries, M. S.; Salem, J. R.; Kiang, C.-H.; Johnson, R. D.; Bethune, D. S. *J. Phys. Chem. A* **1998**, *102*, 2833–2837.

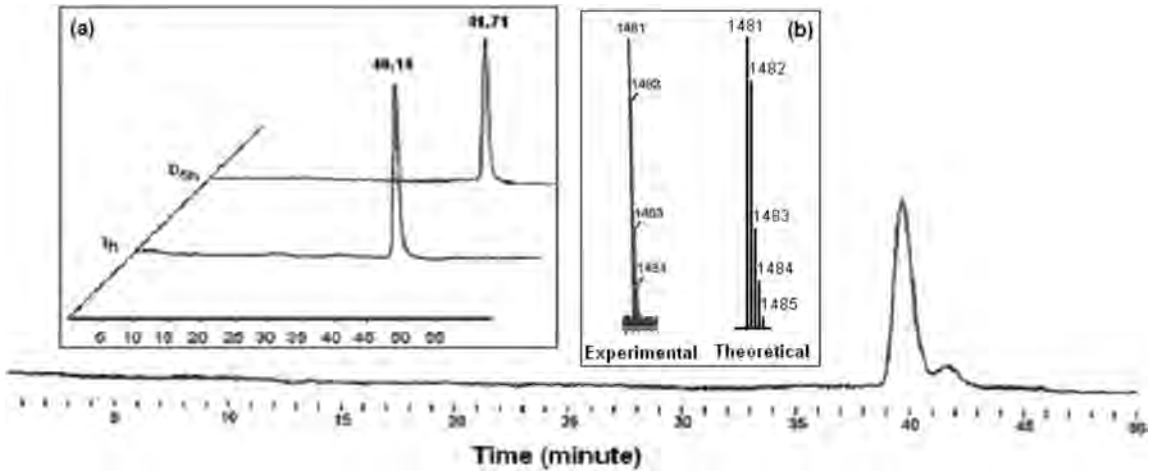

Figure 4. HPLC chromatogram of $Tm_3N@C_{80}$. Two peaks (from left to right) correspond to the two isomers, I_h and D_{5h}, of $Tm_3N@C_{80}$, respectively. The inset parts: (a) HPLC traces of the pure I_h and D_{5h} isomers; (b) Negative ion DCI MS spectrum of the D_{5h} isomer and the calculated isotope distribution for $Tm_3N@C_{80}$. The separation utilized a 5PYE column (10 mm × 250 mm); mobile phase: toluene; flow rate: 2.0 mL/min; detection wavelength: 390nm.

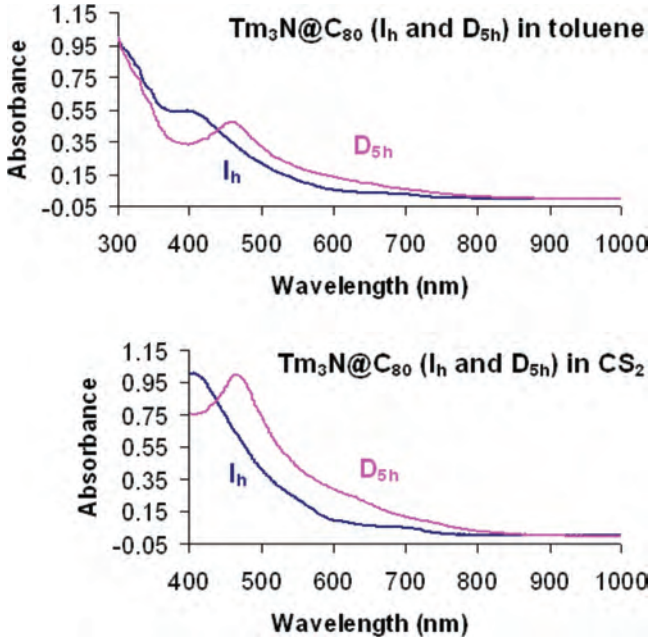

Figure 5. UV−vis spectra of the I_h and the D_{5h} isomers of $Tm_3N@C_{80}$ in toluene or carbon disulfide solution.

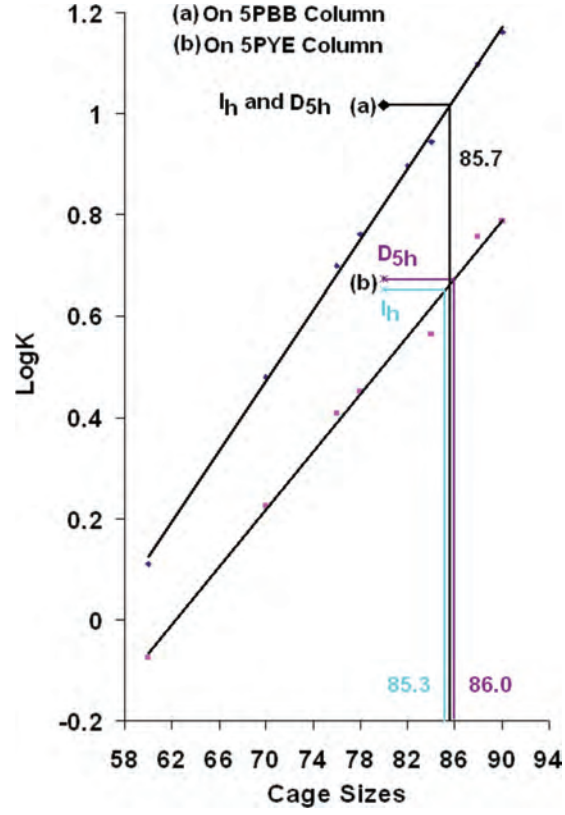

Figure 6. HPLC retention behaviors on the 5PBB and 5PYE columns of the I_h and the D_{5h} isomers of $Tm_3N@C_{80}$. The calibration lines were obtained using log K vs empty fullerene cage sizes from C_{60} to C_{90}. K is the capacity factor of the HPLC column.

the fullerene cage has only 80 carbon atoms. This retention behavior is consistent with a model describing the transfer of six electrons to the cage surface of TNT-EMFs ($[M_3N]^{6+}@C_{80}^{6-}$). Although the PBB column is more sensitive to the polarizabilty of the cage (corresponding total number of π electrons), the 5PYE column is more sensitive to other subtle solute/substrate differences (e.g., dipole moments). Thus, the retention behavior of fullerenes and endofullerenes on a PYE column also depends on the carbon cage shape and polarities. It is this subtle difference that allows these isomers to be separated. This also allows the prediction of a slightly higher induced dipole moment for the D_{5h} isomer in comparison with the I_h isomer.

Crystallographic Structures of $Tm_3N@I_h$-C_{80}·Ni(OEP)·$2C_6H_6$ and $Tm_3N@D_{5h}$-C_{80}·Ni(OEP)·$2C_6H_6$. The crystal structures of $Tm_3N@I_h$-C_{80}·Ni(OEP)·$2C_6H_6$ and $Tm_3N@D_{5h}$-C_{80}·Ni(OEP) ·$2C_6H_6$ are similar with respect to the arrangement of their molecular constituents (fullerene, porphyrin, and benzene), but they are not isostructural. The crystals of $Tm_3N@I_h$-C_{80}·Ni(OEP)·$2C_6H_6$ form in the space group $C2/c$ with $Z = 8$ with no disorder arising from crystallographic symmetry. However, the crystals of $Tm_3N@D_{5h}$-C_{80}·Ni(OEP) form in the space group $C2/m$ with $Z = 4$, which imposes a crystallographic mirror plane on the porphyrin and fullerene portions. In terms of crystal packing, the two structures are alike; their principal difference arises from a superlattice, which removes the mirror disorder in

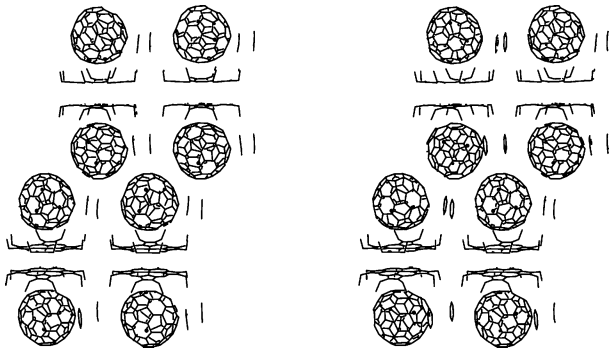

Figure 7. Stereoview of the packing of the molecular constituents in $Tm_3N@I_h$-C_{80}·Ni(OEP).

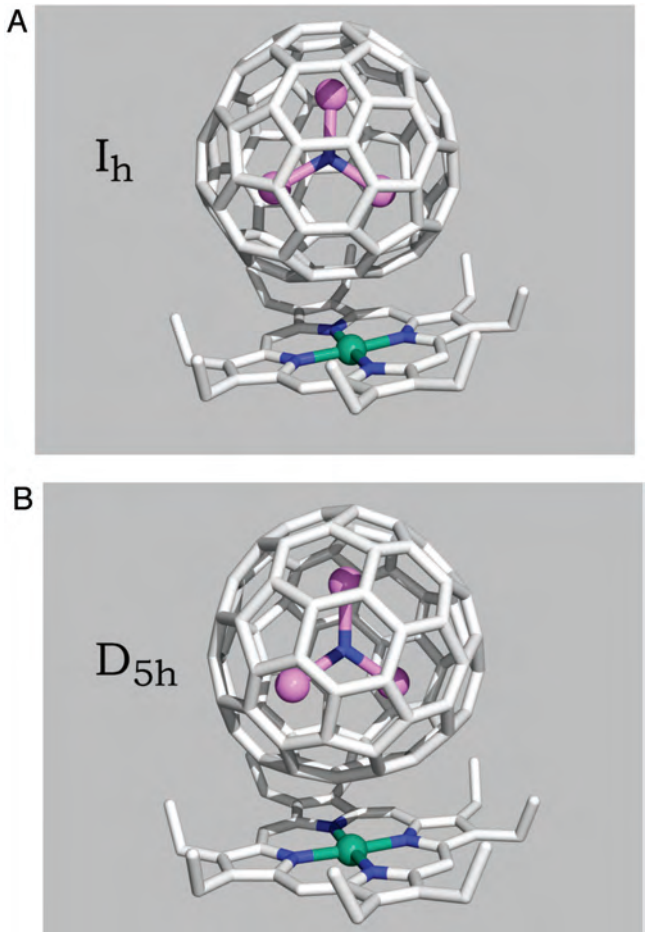

Figure 8. View of the orientation of the endofullerenes with respect to the nickel porphyrin in $Tm_3N@I_h$-C_{80}·Ni(OEP)·$2C_6H_6$ (A) and $Tm_3N@D_{5h}$-C_{80}·Ni(OEP)·$2C_6H_6$ (B). Only the major orientations of the Tm_3N units are shown.

the fullerene portion in the I_h isomer. The other differences result from the differences in the cage symmetries and in how the contents are arranged inside the cages.

A stereoview of the packing of the I_h isomer is shown in Figure 7. This is the structural organization found in both structures, namely, a back-to-back arrangement of Ni(OEP) pairs with fullerene-encapsulating ethyl groups around the periphery of the porpyrin. The closest Ni···Ni distance is 3.447(2) Å in the I_h isomer and 3.470(2) Å in the D_{5h} isomer.

Figure 8 shows the I_h and the D_{5h} isomers with their major set of Tm_3N positions, as they are oriented with respect to

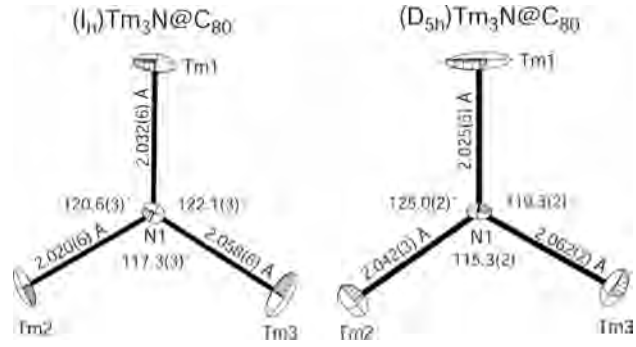

Figure 9. Thermal ellipsoids at the 50% level and the geometry of the predominant Tm_3N set in the I_h and the D_{5h} isomers of $Tm_3N@C_{80}$.

the porphyrin. In all of the $M_3N@C_{80}$ isomers studied to date, this is the arrangement that is found: one of the three metals is distant from the porphyrin, and the other two metal positions lie nearly equidistant from the porphyrin plane. The conservation of this arrangement points out the influence of the external dipolar interactions on the Tm_3N position. The closest contacts between the nickel atom and a carbon atom of the I_h and the D_{5h} isomers are 2.836(8) Å and 2.859(10) Å, respectively. For both structures, the Tm_3N unit is nearly planar. Other geometric details are shown in Figure 9 for the major forms.

Inside the cages, disorder of the Tm_3N occurs. In the case of the I_h isomer, there are two orientations of the trimetallic nitride cluster. The two sets of atoms, (N1, Tm1, Tm2, Tm3) with 67% occupancy and (N1, Tm4, Tm5, Tm6) with 33% occupancy, are individually planar, coplanar to within a dihedral of 7.9°, and rotated with respect to one another around the noncrystallographic 3-fold axis by an average of 17.4°. In the D_{5h} isomer, there is one major set, (N1, Tm1, Tm2, Tm3) with 83% occupancy, and two minor sets, (N1, Tm4, Tm5, Tm6) with 8% occupancy and (N1, Tm7, Tm8, Tm9) with 9% occupancy. The set (N1, Tm4, Tm5, Tm6) is nearly perpendicular to the other two. By considering the internal disorder, it is difficult to identify a preferred orientation of the Tm_3N cluster with respect to the C_{80} cage. However, the orientation of the Tm_3N unit with respect to the C_{80} cage differs in the two isomers, as expected from the difference in symmetry. For example, the 3-fold axis of the (N1, Tm1, Tm2, Tm3) set in the I_h isomer coincides with a 3-fold axis of the C_{80} cage that passes through C12 and C69. Consequently, Tm1, Tm2, and Tm3 have similar η^6 contacts to three hexagons, as shown in the left part of Figure 10. Although this set is only 67% of the total Tm, its impact on the shape of the cage is dramatic. One illustration of this impact can be appreciated by a calculation of the distance from the centroid of the C_{80} to each C atom. For the whole C_{80} cage, the average distance and average deviation is 4.11(5) Å, but the distribution is discontinuous. A set of 18 radii corresponding to the carbon atoms in three hexagons near Tm1, Tm2, and Tm3 have a range of 4.29−4.19 Å, while the remaining carbon atoms have corresponding radii in the range 4.12−4.01 Å. It is as if the three Tm atoms have "punched out" the cage. The average distances and the average deviations for the 18 and 62 radii are 4.23(2) Å and 4.07(2) Å, respectively. Finally,

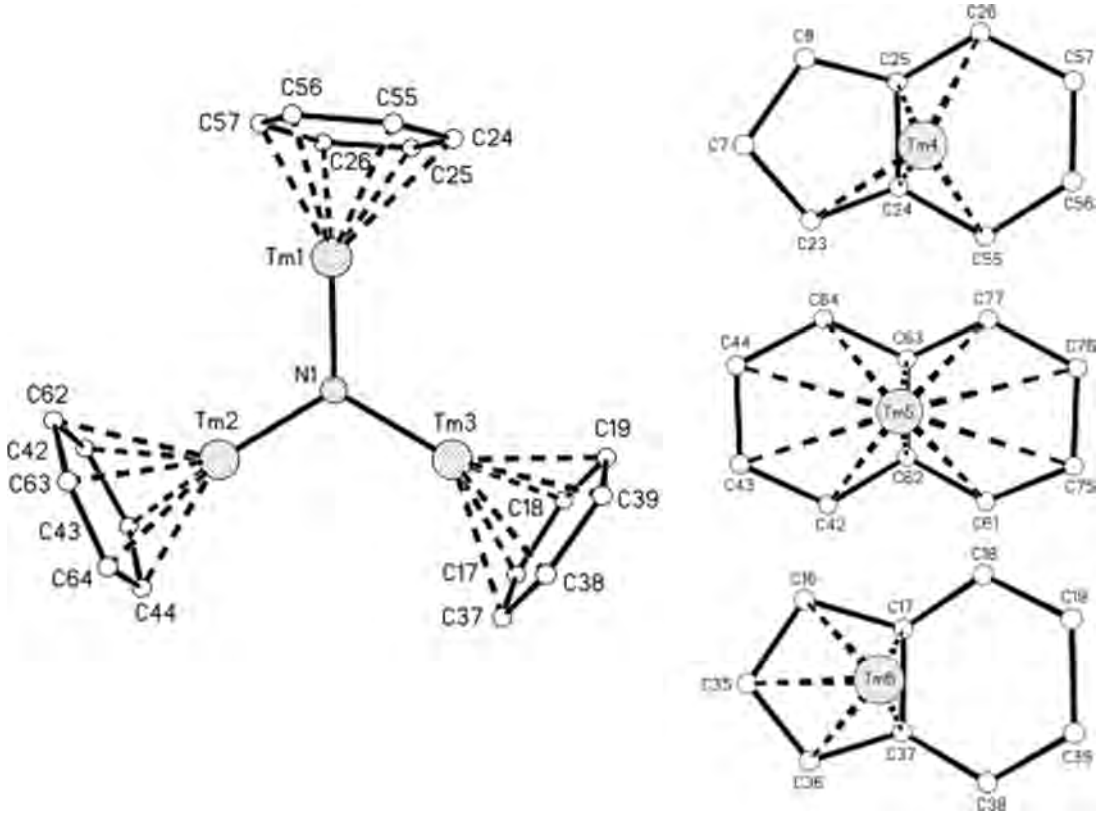

Figure 10. 67% (Tm1, Tm2, Tm3) and 33% (Tm4, Tm5, Tm6) orientations of Tm as viewed from the inside of the C_{80} cage in the I_h isomer. Contact distances: range of six distances in the major orientation of Tm_3N cluster: Tm1, 2.349(10)−2.539(10) Å; Tm2, 2.370(9)−2.528(9) Å; Tm3, 2.357(9)−2.487(9) Å; two closest distances in minor orientation: Tm4−C24, 2.266(10) Å, Tm4−C25, 2.290(9) Å; Tm5−C62, 2.151(10) Å, Tm5−C63, 2.160(10) Å, Tm6−C17, 2.312(10) Å, Tm6−C37, 2.315(9) Å.

we note that the positioning of the Tm atoms at the center of the hexagon is similar to the positioning of the Tb atoms of $Tb_3N@C_{80}$, where again the Tb atoms are located over the six-membered ring of the carbon cage.[20]

Carbon atom contacts less than 2.55 Å for the minor (33%) set, Tm4, Tm5, and Tm6, are shown in the right part of Figure 10. These show more variation, but in each case, there are two shorter contacts that are near 6:6 junctions and two near 6:5 junctions. Notice how the different Tm arrangements nevertheless impact almost the same set of C atoms, reinforcing our view that this is a tight fit.

Figure 11a shows the orientations of the 83% occupancy set of Tm atoms and their closest contacts for the D_{5h} isomer. There is no 3-fold axis of symmetry; thus, the orientation cannot match that of the I_h isomer. This is one of two possible orientations, since there is another set of Tm atoms that are due to the mirror symmetry of the site. Those of the second possibility are depicted in Figure 11b.

Neither arrangement can be ruled out on the basis of bond lengths. Both may occur in the average structure. Just as was true for the I_h isomer, the radius of the D_{5h} fullerene cage appears to be elongated where the close contacts to Tm occur. A similar range of radii, 4.315−4.013 Å, is found with an average radius and an average deviation of 4.11(5) Å. In the D_{5h} case, the distribution of radii is more continuous, falling off sharply at first and then leveling off until it dips at the smallest values. The shortest radii (for both isomers) are in the region where the fullerene encounters the porphyrin plane. Very similar impressions about the distortions away from spherical that are caused by the Tm_3N unit can be obtained in another manner: the pyramidalization angles (ϕ_p) at each C of the cage according to the POAV3 method of Haddon.[46] In this method, an sp^2 carbon has $\phi_p = 0°$, while an sp^3 carbon has $\phi_p = 19.47°$. On the basis of our calculations, the angle found for any carbon atom with a thulium atom less than approximately 2.55 Å away is clearly affected by a close metal contact. For the I_h isomer, type "A" carbons have an average ϕ_p of 8.8(4)° and 10.9(4)° for those distant and near to Tm, respectively; for type "B" carbons, the values are 9.9(7)° and 11.5(10)°, respectively. Thus, there are clear trends that carbon atoms at the intersection of three hexagons are more sp^2-like, and carbon atoms near Tm are more pyramidalized and more sp^3-like. It is interesting to note that the carbon nearest to the porphyrin is less pyramidalized than would be expected for its type.

Figure 12 shows the relative orientations of the M_3N units relative to the idealized 5-fold axis of the D_{5h} cage in three different endofullerenes: $Sc_3N@D_{5h}$-C_{80}, $Tm_3N@D_{5h}$-C_{80}, and $Tb_3N@D_{5h}$-C_{80}. The variability in the position of the major set of M_3N atoms inside the C_{80} cage is evident in this view. In addition, the deviation from planarity of the M_3N unit increases from left to right. The angle between the M_3N plane and the 5-fold axis (vertical, in the plane of the paper) and the perpendicular displacement of N1 from the M_3N plane are 59.4° with $\Delta N1 = 0.029$ Å for $Sc_3N@C_{80}$,

(46) Haddon, R. C.; Raghavachari, K. In *Buckminsterfullerenes*; Billups, W. E., Ciufolini, M. A., Eds.; VCH: New York, 1993; Chapter 7.

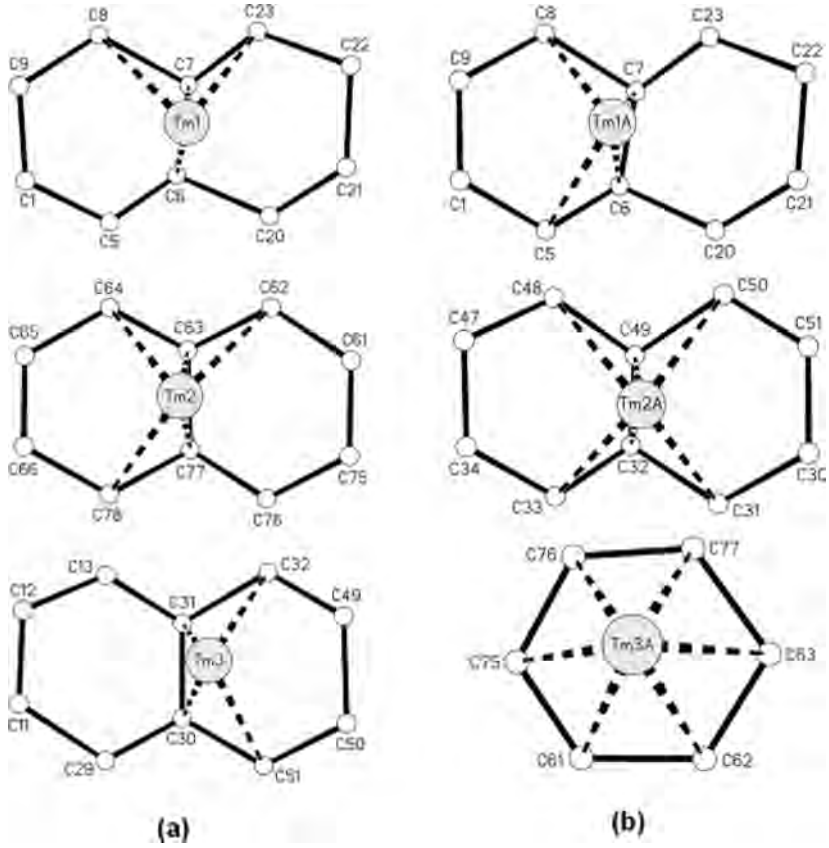

Figure 11. (a) Orientations of the 83% set (Tm1, Tm2, Tm3) as viewed from the inside of the C_{80} cage in the D_{5h} isomer. Contact distances between Tm and C less than 2.55 Å are shown with dashed lines. The shortest two distances are as follows: Tm1−C6, 2.345(12) Å, Tm1−C7, 2.267(13) Å; Tm2−C63, 2.253(11) Å, Tm2−C77, 2.256(12) Å; Tm3−C30, 2.25(2) Å, Tm3−C31, 2.198(16) Å. (b) Orientations of the mirrored 83% set (Tm1a, Tm2a, Tm3a) as viewed from the inside of the C_{80} cage in the D_{5h} isomer. Contact distances between Tm and C less than 2.55 Å are shown with dashed lines. The shortest two distances for Tm1a and Tm2a are as follows: Tm1a−C7, 2.305(13) Å, Tm1a−C6, 2.345(12) Å; Tm2a−C32, 2.257(17) Å, Tm2a−C49, 2.318(13) Å. The range of six distances for Tm3a is 2.340(12)−2.511(12) Å.

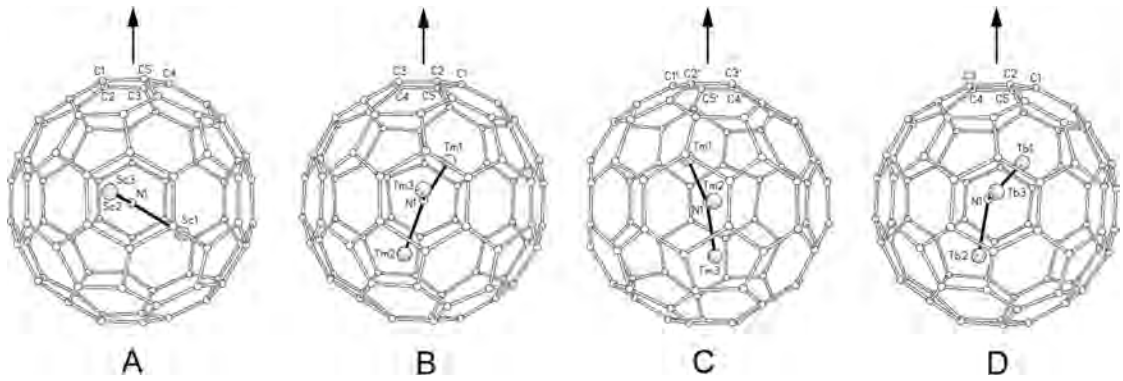

Figure 12. Orientations of the major set of M_3N atoms inside the D_{5h}-C_{80} cage: (A) $Sc_3N@D_{5h}$-C_{80}; (B and C) $Tm_3N@D_{5h}$-C_{80}; (D) $Tb_3N@D_{5h}$-C_{80}. There are two views for $Tm_3N@C_{80}$ because there are two equally populated orientations of the cage present. In each drawing, the location of the 5-fold axis of the idealized cage is denoted by the arrows.

23.0° and 15.5° with ΔN1 = 0.082 Å for the two orientations of $Tm_3N@C_{80}$, and 21.7 ° with ΔN1 = 0.416 Å for $Tb_3N@C_{80}$.

Magnetic Properties of $Tm_3N@I_h$-C_{80}. We have measured the magnetic susceptibility of a 3.1 mg sample of $Tm_3N@I_h$-C_{80} and found results that contrast with those reported previously for $Ho_3N@C_{80}$ and $Tb_3N@C_{80}$.[38] As seen in Figure 13, the χT versus T data can be fit to a Curie−Weiss law with $C = 23.4$ emu·K/mol, consistent with the calculated value for three uncoupled Tm^{3+} ions considering the spin and orbital contributions with no quenching of the orbital angular momentum ($L = 5$, $S = 1$, and $J = 6$; $C_{calcd} = 23.3$ emu·K/mol). The θ value is −88 K, indicating antiferromagnetic coupling between the spins. Interestingly, the χT appears to be tending toward 0 emu·K/mol at low temperature. This might indicate that, in the ground state, the spin vectors are aligned along the Tm−N bonds here as well, but all radiating away from or toward the nitrogen atom, yielding a net diamagnetic ground state. The M versus H plot (Supporting Information), measured at 1.8 K, indicates simple paramagnetic behavior up to 7 T with no evidence of saturation. This is not surprising considering the large

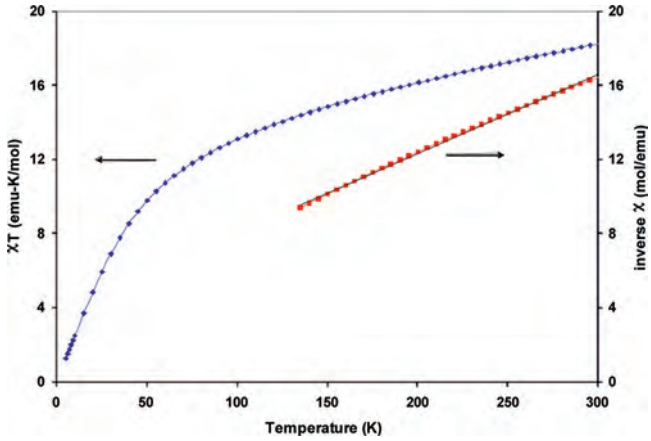

Figure 13. Measurements of magnetic properties of $Tm_3N@I_h$-C_{80}.

orbital contribution to the moment. The data show slight curvature near 0 G, but this can be explained by a slight ferromagnetic impurity.

To further investigate the nature of the apparent antiferromagnetic interactions, we have made a solid solution of $Tm_3N@I_h$-C_{80} in C_{60} in roughly a 1:9 ratio by dissolving each in CS_2 and removing the solvent. We assume that, because very similar van der Waals interactions should exist between the two compounds, the distribution should be uniform, leaving the $Tm_3N@C_{80}$ molecules dispersed in C_{60} such that the intermolecular magnetic coupling between the $Tm_3N@C_{80}$ molecules should be decreased substantially. The χT versus T for this sample, scaled to moles of Tm compound (C_{60} is diamagnetic) and corrected for the diamagnetism of the C_{60}, exhibits the same shape and essentially the same Curie−Weiss theta (θ). We interpret this to indicate that the antiferromagnetic coupling is intramolecular.

Electrochemical Properties of the I_h and the D_{5h} Isomers of $Tm_3N@C_{80}$. Electrochemical experiments were carried out on isomerically pure I_h and D_{5h} $Tm_3N@C_{80}$ samples. Cyclic voltammograms (CVs) at a scan rate of 100 mV/s of both isomers (Figure 14a) show electrochemically irreversible reductions and quasireversible oxidations. Increasing the scan rate up to 30 V/s did not improve the reversibility of the reduction waves. An examination of the first reductions of both isomers shows them to occur at almost identical potentials (−1.43 V for the I_h isomer and −1.45 V for the D_{5h} isomer), while their first oxidation potentials are +0.65 V for the I_h isomer and +0.39 V for the D_{5h} isomer. The electrochemical (HOMO−LUMO) gap of the I_h and the D_{5h} isomers of $Tm_3N@C_{80}$ are 2.08 and 1.84 V, respectively. These gaps are very similar to those of $Lu_3N@C_{80}$ isomers (2.04 V for the I_h isomer and 1.86 V for the D_{5h} isomer),[17] while they are significantly larger than those of the $Sc_3N@C_{80}$ isomers (1.84 V for the I_h isomer and 1.67 V for the D_{5h} isomer).[17] Osteryoung square wave voltammetry (OSWV) of the separated isomers (Figure 14b) shows both have a high degree of purity, since no appreciable current is detected for the missing isomer, although a trace of the D_{5h} isomer can be seen in the voltammogram of the I_h sample in Figure 14b. As in the case of $Sc_3N@C_{80}$, the first two oxidations of the D_{5h} isomer of $Tm_3N@C_{80}$, at 0.39 and 0.78

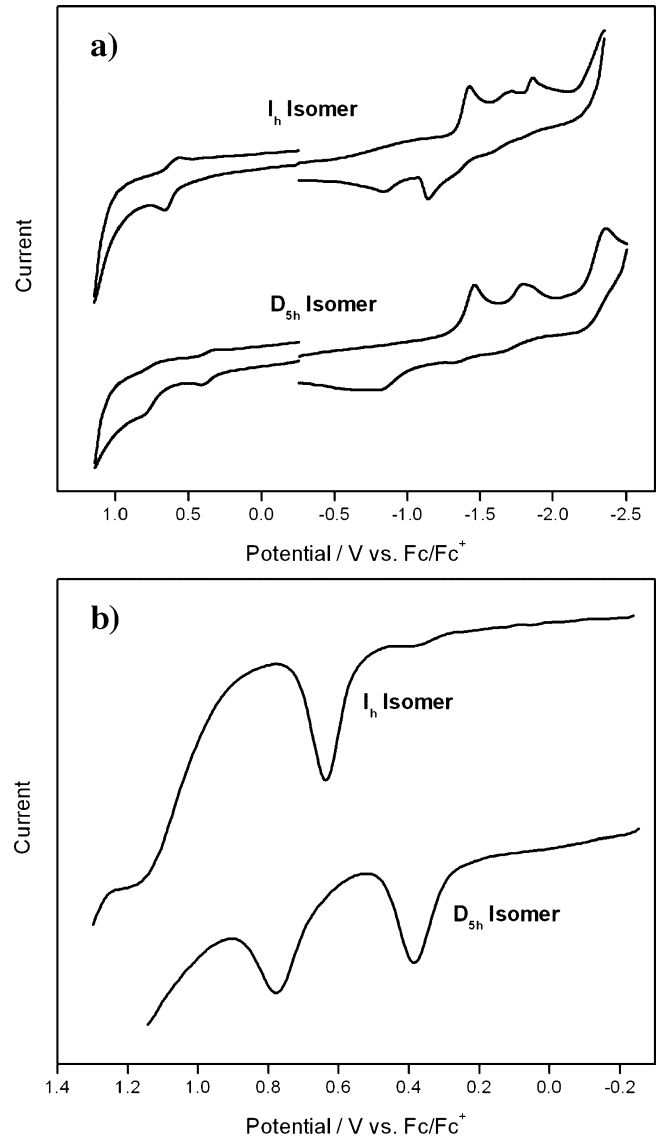

Figure 14. (a) CV of the I_h and the D_{5h} isomers of $Tm_3N@C80$; (b) OSWV of the oxidations of the I_h and the D_{5h} isomers of $Tm_3N@C_{80}$.

Table 1. Redox Potential (V) and Electrochemical Gap (V)

compd	$^{red}E_1$	$^{ox}E_1$	$^{ox}E_1 - {}^{red}E_1$
$Tm_3N@I_h$-C_{80}	−1.43	+0.65	2.08
$Tm_3N@D_{5h}$-C_{80}	−1.45	+0.39	1.84
$Lu_3N@I_h$-C_{80}[17]	−1.40	+0.64	2.04
$Lu_3N@D_{5h}$-C_{80}[17]	−1.41	+0.45	1.86
$Sc_3N@I_h$-C_{80}[17]	−1.27	+0.57	1.84
$Sc_3N@D_{5h}$-C_{80}[17]	−1.33	+0.34	1.67
$Sc_3N@I_h$-C_{80}[47]	−1.22	+0.62	1.84
$Sc_3N@I_h$-C_{80}[48]	−1.24	+0.62	1.86
$Sc_3N@I_h$-C_{80}[49]	−1.26	+0.59	1.89

V, are separated by a smaller potential difference (0.39 V) than those of the corresponding I_h isomer (0.53 V). Table 1 shows the redox potentials and HOMO−LUMO gaps for the isomerically pure I_h and D_{5h} $Tm_3N@C_{80}$ samples.

(47) Iiduka, Y.; Ikenaga, O.; Sakuraba, A.; Wakahara, T.; Tsuchiya, T.; Maeda, Y.; Nakahodo, T.; Akasaka, T.; Kako, M.; Mizorogi, N.; Nagase, S. *J. Am. Chem. Soc.* **2005**, *127*, 9956–9957.
(48) Dunsch, L.; Krause, M. *ChemPhysChem* **2004**, *5*, 1445–1449.
(49) Elliott, B.; Yu, L.; Echegoyen, L. *J. Am. Chem. Soc.* **2005**, *127*, 10885–10888.

Conclusions

The I_h and the D_{5h} isomers of $Tm_3N@C_{80}$ can be prepared by conducting the modified Krätschmer−Huffman electric-arc in the presence of dinitrogen. An efficient method of purification of the two isomers has been developed, and the structures of both isomers have been determined by X-ray crystallography. The χT versus T data for $Tm_3N@I_h$-C_{80} have been fit to the Curie−Weiss law with $C = 23.4$ emu·K/mol, which is consistent with the calculated value for three uncoupled Tm(III) ions. The electrochemical measurements demonstrate that both the I_h and the D_{5h} isomers of $Tm_3N@C_{80}$ have a large HOMO−LUMO gap, similar to those of other C_{80}-caged TNT-EMFs.

Experimental Section

Synthesis of $Tm_3N@C_{80}$. The core-drilled graphite rods (6.4 mm diameter) were packed with a mixture of Tm_2O_3, graphite powder, and iron nitride according to a weight ratio of 2.1:1.0:0.4, respectively. The rods were packed in a 3 mm recessed form. The packed rods were preheated at about 1000 °C in a dinitrogen flow for about 10 h. The recessed rods were statically vaporized in a Krätschmer−Huffman arc-discharge fullerene generator with a total pressure of 300 torr including 20 torr dinitrogen and 280 torr helium. The direct electric current and voltage were set at 105 A and 30 V, respectively. The fullerene containing soot was collected in a thimble and extracted in a Soxhlet extractor using toluene as the solvent for about 20 h to obtain the extract.

Chemical Separation. The extract or soot in toluene was placed on the CPDE-MPR column and allowed to slowly pass through it. The flow rate was about 20 mL/h. The elutant was continuously collected for 48 h. Then, the solvent evaporated to obtain a concentrated solution of PAHs and $Tm_3N@C_{80}$ isomers.

Washing out the PAHs. The solution containing the PAHs and $Tm_3N@C_{80}$ isomers was evaporated under a stream of dinitrogen in a centrifuge tube. Acetone was added to the centrifuge tube to dissolve the PAHs. The tube was capped with a cork and sonicated for 5 min. After the sonication, the suspension was centrifuged for 5 min. The supernatant (containing the PAHs) was carefully removed from the centrifuge tube. Then, the sonication, washing, and centrifugation steps were repeated two more times.

Crystal Growth. Crystals of each isomer of $Tm_3N@C_{80}$·Ni(OEP)·$2C_6H_6$ were obtained in a glass tube by layering a brown solution of approximately 0.5 mg of the appropriate isomer of $Tm_3N@C_{80}$ in 0.5 mL of benzene over a red saturated solution of Ni(OEP) in benzene solution. The glass tube was placed in a homemade device to avoid the disturbances of light, magnetic field, and vibration. Over a period of about 14 days, the two layers diffused together at room temperature. Finally, the mother liquid was decanted, and the small, black parallelepiped crystals were harvested.

X-ray Structure Determinations.

$Tm_3N@I_h$-C_{80}·Ni(OEP)·$2C_6H_6$. A black parallelepiped of dimensions $0.03 \times 0.06 \times 0.07$ mm^3 was mounted in the 90(2) K nitrogen cold stream provided by a CRYO Industries low temperature apparatus on the goniometer head of a Bruker SMART Apex diffractometer equipped with an ApexII CCD detector. Diffraction data were collected with graphite-monochromated Mo Kα radiation employing a 0.3° ω scans and approximately a full sphere of data to $2\theta_{max}$ of 63°. A multiscan correction for absorption was applied using the program SADABS 2.10. Upon inspection of the scattering intensities, the data was truncated to $2\theta = 55°$, yielding a total of 97 085 reflections collected, of which 17 151 were unique [R(int) = 0.078] and 12 600 were observed [$I > 2\sigma(I)$]. The structure was solved by direct methods (SHELXS-97) and refined by full-matrix least-squares on F^2 (SHELXL97) using 1269 parameters. There are two sets of three Tm's in the interior of the C_{80} cage, (Tm1, Tm2, Tm3) and (Tm4, Tm5, Tm6). Their occupancies were initially determined by refinement and were subsequently fixed at their refined values of 0.67 and 0.33 for the two sets, respectively. All non-hydrogen atoms were refined with anisotropic thermal parameters. The H atoms on C atoms were generated geometrically and refined as riding atoms with C−H = 0.95−0.99 Å and U_{iso}(H) = 1.2 times U_{eq}(C) for CH and CH_2 groups and U_{iso}(H) = 1.5 times U_{eq}(C) for CH_3 groups. The maximum and minimum peaks in the final difference Fourier map were 2.27 and −2.47 eÅ^{-3}. This residual density probably corresponds to an additional minor (<4%) Tm atom position. Crystal data is as follows: $C_{128}H_{56}N_5NiTm_3$, M_w = 2229.28, monoclinic, $C2/c$, $a = 44.8763(16)$ Å, $b = 15.0510(5)$ Å, $c = 25.3167(9)$ Å, $\beta = 118.993(4)°$, $V = 14956.8(11)$ Å^3, T = 90(2) K, $Z = 8$, R_1 [$I > 2\sigma(I)$] = 0.0665, R_2 (all data) = 0.1561, GOF (on F^2) = 1.118.

$Tm_3N@D_{5h}$-C_{80}·Ni(OEP)·$2C_6H_6$. The details correspond to those of the I_h isomer above. A black parallelepiped of dimensions $0.04 \times 0.07 \times 0.10$ mm^3 was used for data collection, and the data were truncated to $2\theta_{max}$ of 55°, yielding a total of 42 936 reflections collected, 8913 independent reflections [R(int) = 0.033] and 7470 observed reflections [$I > 2\sigma(I)$]. A total of 635 parameters was used in the refinement. For the porphyrin, the crystallographic mirror corresponds with the molecular symmetry. However, the fullerene, with a point group symmetry of D_{5h}, does not utilize any of its mirror planes in its placement in the unit cell. Consequently, the solution of the structure of the fullerene portion requires that two superimposed cages need to be sorted out, but fortunately, in this case, there is only one orientation of the cage once the mirror symmetry is taken into account. Refinement converged well with a set of 80 C atoms, all at 0.5 occupancy, and the use of the PART −1 statement on SHELXL97. There is also disorder with respect to the Tm atoms. This disorder was modeled with three sets of three Tm positions, all with a common central N, and with refined occupancies constrained to 0.50000(1) and final occupancy values of 0.4135(10), 0.0397(6), and 0.0466(12). Only the major set, comprised of Tm1, Tm2, and Tm3, was assigned anisotropic thermal ellipsoids. Maximum and minimum residuals were 2.12 and −1.51 eÅ^{-3}, respectively. Crystal data is as follows: $C_{128}H_{56}N_5NiTm_3$, $M_w = 2229.28$, monoclinic, $C2/m$, $a = 25.2777(5)$ Å, $b = 15.0945(3)$ Å, $c = 19.6748(4)$ Å, $\beta = 95.483(2)°$, V = 7472.7(3) Å^3, $T = 90(2)$ K, $Z = 4$, R_1 [$I > 2\sigma(I)$] = 0.0575, R_2 (all data) = 0.1604, GOF (on F^2) = 1.091.

Measurement of Magnetic Properties. All the magnetic measurements were performed on a 7 T Quantum Design MPMS SQUID magnetometer. The measurements of magnetization as a function of temperature were performed from 1.8 to 300 K in a 5000 G applied field as indicated. Randomly oriented polycrystalline samples were cooled in a zero applied field and measured upon warming. Samples were packed between cotton plugs and measured in gelatin capsules.[50] Diamagnetic corrections were applied for the cotton, the gelatin, and for the core diamagnetism based on Pascal's constants for $\chi^T(T)$ plots.

Electrochemical Measurements. All CV and OSWV experiments were carried out in a one-compartment cell in a solution of *o*-dichlorobenzene containing 0.1 M (t-Bu)$_4$NPF$_6$ using a standard three electrode arrangement. A Pt disk (1 mm) was used as the working electrode, a Pt wire was used as the auxiliary, and a Ag wire in a 0.01 M $AgNO_3$/0.1 M (t-Bu)$_4$NPF$_6$ CH_3CN solution was

used as the reference electrode. Ferrocene was added to the solution at the end of each experiment to act as an internal reference, and all electrochemical potentials (measured from OSWV) were referenced to its redox couple.

Acknowledgment. We are grateful for the support of this work by the National Science Foundation [(CHE-0716843 (A.L.B. and M.M.O.) and CHE-0413857 (A.L.B.), CHE-043700 (H.C.D.), DMR-0507083 (H.C.D., H.W.G.)] and by the National Institute of Health [1R01-CA119371-01 (H.C.D., H.W.G.)].

Supporting Information Available: Crystallographic data in CIF format and atomic numbering schemes for $Tm_3N@I_h$-C_{80}·Ni(OEP)·$2C_6H_6$ and $Tm_3N@D_{5h}$-C_{80}·Ni(OEP)·$2C_6H_6$, HPLC chromatograms and DCI MS spectrum of the extracts of the dinitrogen method, view and thermal ellipsoid drawings of D_{5h} isomer, and plot of the magnetic moment of $Tm_3N@I_h$-C_{80} versus magnetic field. This material is available free of charge via the Internet at http://pubs.acs.org.

IC800227X

(50) Sellers, S. P.; Korte, B. J.; Fitzgerald., J. P.; Reiff, W. M.; Yee, G. T. *J. Am. Chem. Soc.* **1998**, *120*, 4662–4670.